Available online at www.sciencedirect.com
SCIENCE DIRECT®
Scripta Materialia 51 (2004) 887–891
Scripta MATERIALIA
www.actamat-journals.com

Prediction of stress directionality from pile-up morphology around remnant indentation

Yun-Hee Lee [a,b,*], Kazuki Takashima [a], Yakichi Higo [a], Dongil Kwon [b]

[a] *Precision and Intelligence Laboratory, Tokyo Institute of Technology, 4259 Nagatsuta, Midori-ku, Yokohama 226-8503, Japan*
[b] *School of Materials Science and Engineering, Seoul National University, San 56-1, Gwanak-gu, Seoul 151-742, Korea*

Received 6 April 2004; received in revised form 16 June 2004; accepted 28 June 2004
Available online 20 July 2004

Abstract

The directionality and magnitude in surface stress was scrutinized from non-symmetrical morphology of Brale indenting deformation on artificially strained specimen. A non-equibiaxial stress applied brought about different pile-up variations along two orthogonal straining axes and the asymmetric deformation behavior was related with a ratio of its two principal stress components.

Keywords: API X65 steel; Indentation; Residual stresses; Pile-up morphology

1. Introduction

Numerous indentation approaches [1–3] have been conducted over the past few decades for the characterization of preexisting surface stress. A tensile stress applied enhances shear plasticity beneath Vickers [1,2] or Rockwell indenter [3], thereby increasing indentation depth and reducing hardness. The alteration in hardness by the stress application was, however, less than 10% of the intrinsic hardness in unstressed state. Tsui et al. and Bolshakov et al. [4,5], studying an influence of surface stress on contact morphology, reported that the contact area was invariant at a fixed load regardless of the elastic applied stress. By adopting this as a basic assumption, a series of theoretical models [6,7] have been proposed to analyze a stress-induced shape change in instrumented indentation curve. Suresh and Giannakopoulos [6] predicted an average surface stress from the difference in indentation load of the stressed and unstressed specimens. Their model, however, underestimated the surface stress because a shear-deformation-independent hydrostatic stress part was not excluded to derive a stress contribution to the plastic deformation. Thus Lee and Kwon [7] modified the model by deriving a stress-induced normal pressure additive to the contact pressure from a shear deviatoric stress part, obtained by removing the hydrostatic stress part from the surface stress. Swadener et al. [8] investigated a stress dependency of spherical indenting deformation and proposed an initial yielding pressure as a stress indicator.

The current indentation models [6–8], however, have some limitations, obstructing their applications for such actual components as joined parts, mechanically machined surface, and surface coating. The limitations are that the indenters used probe an averaged response of the surface stress [9] and that a structurally equivalent unstressed specimen is indispensable to separate the stress contribution from a whole indenting deformation on a stressed specimen [10]. According to Vickers indentation results on biaxially stressed specimens [11], if information on a stress ratio of two principal

* Corresponding author. Address: Precision and Intelligence Laboratory, Tokyo Institute of Technology, 4259 Nagatsuta, Midori-ku, Yokohama 226-8503, Japan. Tel./fax: +81 45 924 5631.
E-mail address: uni44@mmrl.snu.ac.kr (Y.-H. Lee).

1359-6462/$ - see front matter
doi:10.1016/j.scriptamat.2004.06.034

components is provided, individual principal stress can be derived from the average stress. This stress simulation test is also free from the limitation on reference stress-free specimen. Thus the stress ratio became an important issue in the stress characterization and a non-symmetrical contact deformation in uniaxial stress, observed by Underwood [12], supplied a clue of extracting the directionality in surface stress. We tried to estimate the stress directionality by performing Brale indentations on biaxially strained specimens and by analyzing the amount and anisotropy in pile-up morphologies around the impressions from a viewpoint of the stress ratio in the biaxial stresses applied.

2. Experimental details

15-mm-thick rectangular beam and cross-shaped specimens, cut from a small-grained API X65 steel plate, were heat-treated at 600 °C for 2 h to remove internal stress and then their surfaces were polished with 0.5 μm alumina powder (see Fig. 1(a)). A stress-generating apparatus, having two independent orthogonal loading axes, was designed for the generation of biaxial stress. The specimen was tightened inside of the apparatus and was strained elastically using bending screws, as shown in Fig. 1(b). To keep the applied strain below the elastic limit, the difference in two orthogonal principal strain components was maintained below the specimen yield strain according to the Tresca yield criterion. Detailed information on the devised apparatus and straining procedure can be referred from Ref. [11]. Surface strains, simulated on the specimens, were converted to elastic uniaxial and biaxial stresses using the Young's modulus 210 GPa and Poission's ratio 0.3 of the API X65 steel. Indentation tests on the elastically bent specimens were carried out with an AIS 3000R system (made by Frontics, Inc., Seoul, Korea) whose load and depth resolutions were 0.02 N and 0.10 μm, respectively. The indentation test was repeated 5 times with a peak load 294 N and indenting speed 0.2 mm/min. Stress relaxation about 2.1 MPa at the peak load was negligible compared to the applied stress. A circular cone shape of the Brale impression allowed us to detect a biaxial stress-induced non-symmetrical surface deformation easily. Top and cross-sectional morphologies of the remnant impression were observed using a co-focal 1LM21W laser microscope (made by Lasertec Corp., Yokohama, Japan) with a displacement resolution 0.3 μm. The cross-sectional impression profiles were measured along radial lines parallel to the two orthogonal loading axes. The Brale indentations were also carried out on the unstressed specimen to compare their deformation patterns with those of the stressed specimen.

3. Results and discussion

3.1. Surface deformation around Brale indentation on API X65 steel specimen

The indentation invoked a peak penetration depth 86.1 ± 0.2 μm and remnant circular impression 438.7 ± 2.0 μm in a diameter on the unstressed specimen. Local surface near the impression is bulged and its detailed morphologies, observed from the surface-normal and lateral directions, show a nearly circular symmetric pile-up deformation regardless of the measuring direction (see Fig. 2). Width and height are proposed as two parameters, measuring a degree of the material accumulation. Since a far-ridge of the pile-up converged slowly to the undeformed specimen surface, a boundary of surface deformation was ambiguous and the measured pile-up width 288.4 ± 6.2 μm also showed a significant standard deviation. While the height parameter showed a less scattering behavior of 15.3 ± 1.6 μm but two pile-up profiles, measured on opposite sides of an

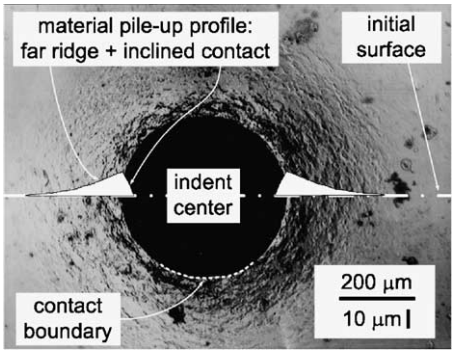

Fig. 2. Top and cross-sectional views of three-dimensional morphology of a Brale indentation on the unstressed API X65 steel specimen.

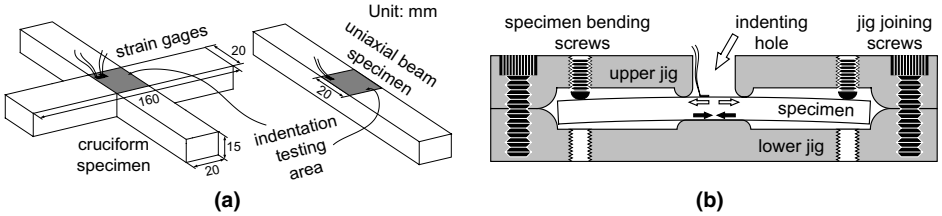

Fig. 1. Schematic diagrams of (a) cruciform and rectangular beam specimens and (b) bending apparatus for artificial straining.

impression diameter, could display a little discrepancy due to an oblique contact, might be made on an unflatly ground specimen. A mean of the asymmetric pile-up heights was, however, consistent with the symmetric one and a trajectory of peak points in several profiles around an impression formed a contact boundary (see Fig. 2). Thus the pile-up height is used in subsequent experiments as an empirical parameter, describing the surface morphology of the remnant indentation.

3.2. A dependency of pile-up height on a magnitude of applied stress

Eight stress states, applied on the cross-shaped and beam specimens in Fig. 1(a), were divided into four categories of uniaxial ($\sigma_x^{app} \neq 0, \sigma_y^{app} = 0$: #3 and 6), equi-biaxial ($\sigma_x^{app} = \sigma_y^{app} \neq 0$: #1 and 8), biaxial ($\sigma_x^{app} \neq \sigma_y^{app} \neq 0$: #2, 5, and 7), and pure shear ($\sigma_x^{app} = -\sigma_y^{app} \neq 0$: #4) states (see Table 1). When an axial stress, higher than its orthogonal stress component in an absolute value, is denoted as a major principal stress σ_x^{app}, every surface stress can be expressed using a ratio of two axial stress components κ or $\sigma_y^{app}/\sigma_x^{app}$, where σ_y^{app} is a minor principal stress [11]. A fluctuation in the remnant contact diameter by the stress application was less than 1.75% of its value in the unstressed specimen and this confirms that the contact area is independent of the elastic surface stress [4,5]. The peak penetration depth h_{max}, however, had a unique value for each stress state and its deviating amount Δh_{max} from that in the unstressed state was proportional to the average of applied stress (see Fig. 3). The average applied stress in tensile state produced Δh_{max} with a positive sign and this was explained from its enhancement of the Mises stress and shear plasticity beneath the indenter. Symmetrically opposite response of the compressive average stress also could be explained by the same arguments.

In order to scrutinize the influences of biaxial applied stress on the pile-up response, a stress-induced shift in the pile-up height Δh^{pile} was obtained from the difference

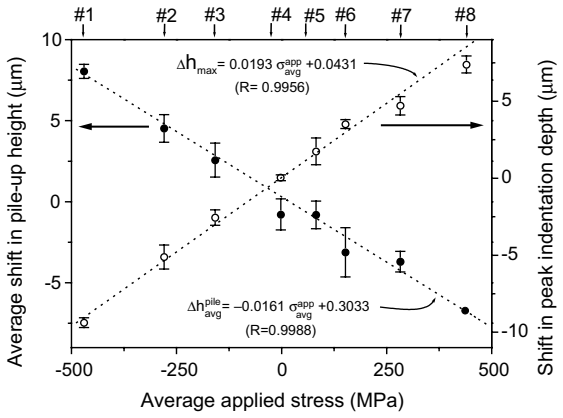

Fig. 3. Empirical dependencies of the stress-induced variations in pile-up height and peak indentation depth on the applied average stress.

in pile-up height of the stressed and unstressed specimens. Δh_x^{pile} and Δh_y^{pile}, measured along the major and minor loading axes, showed different values in the applied stress states excepting #1 and 8 in the equi-biaxial state and this inhomogeneous material accumulation was explained with a combination of pile-up enhancing and reducing roles of the uniaxial compressive and tensile stresses, respectively, at impression edges perpendicular to the straining axis. The large scattering in pile-up height in #4 and other specimens are explained with the influence of asymmetric pile-up data from opposite sites of the impression along one profile measuring line. If raw data measured from the left and right parts of the impression are not averaged, an actual standard deviation will be less than ±0.8 μm. Δh_x^{pile} and Δh_y^{pile} were averaged into a representative pile-up measurement Δh_{avg}^{pile} for each stress state. Δh_{avg}^{pile} shows a reverse proportional dependency on the average applied stress σ_{avg}^{app} in Fig. 3 because an upward pile-up deformation occurs when indented material cannot be accommodated by the elastic/plastic deformation beneath an indenter any more. Thus a large pile-up deformation is often observed from remnant impression in a compressive surface stress, constraining the indenting plasticity (Fig. 4).

Table 1
Artificially generated eight stress states and their resultant pile-up morphologies

Stress state	Major axial stress σ_x^{app} (MPa)	Stress ratio κ	Average applied stress σ_{avg}^{app} (MPa)	Pile-up height shift of major axis Δh_x^{pile} (μm)	Pile-up height shift of minor axis Δh_y^{pile} (μm)
#1	−470.7	1.0	−470.3	8.0 ± 0.6	8.1 ± 1.9
#2	−377.8	0.48	−279.5	3.8 ± 1.0	5.3 ± 1.9
#3	−316.3	0	−158.1	1.6 ± 2.5	3.5 ± 0.8
#4	−228.1	−0.99	−1.7	−1.6 ± 0.8	0.0 ± 2.9
#5	267.5	0.39	81.9	−0.3 ± 2.5	−1.4 ± 1.1
#6	303.7	0	151.8	−1.7 ± 2.5	−4.5 ± 0.5
#7	372.3	0.52	282.6	−3.2 ± 1.3	−4.2 ± 2.7
#8	444.3	0.98	439.8	−6.8 ± 2.3	−6.8 ± 0.9

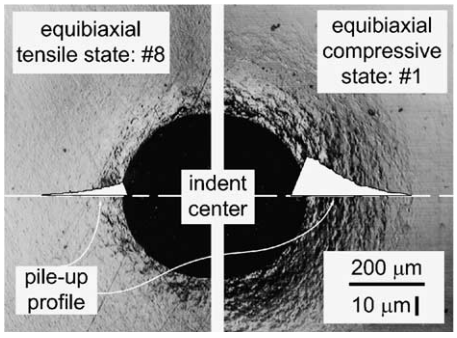

Fig. 4. Comparison of the pile-up deformations in tensile and compressive equi-biaxial stress states.

3.3. A dependency of pile-up height ratio on a directionality of applied stress

Similar with the definition of stress ratio, a stress-induced pile-up shift ratio along the two loading axes or $\Delta h_y^{\text{pile}}/\Delta h_x^{\text{pile}}$ is proposed a parameter, probing the stress directionality in the indented region. $\Delta h_y^{\text{pile}}/\Delta h_x^{\text{pile}}$ data, measured from the eight stress states, are plotted against the stress ratio in Fig. 5 and are fitted into a linear function of κ for API X65 steel specimen. This relationship would be applicable for some metallic materials, having similar work-hardening behavior with that of API X65 steel. In addition it needs a micromechanical modeling on the pile-up behavior and its stress dependency to derive a general function covering the whole metallic materials from the empirical fitting relationship in Fig. 5. A slope of the fitting line is 0.53 and it means that a change rate in the stress-induced pile-up shift ratio is nearly half of that in the stress ratio. A uniaxial compressive stress enhances an upward surface displacement around whole Brale impression and additively invokes the upward pile-up and downward compressive deformations, respectively, at the impression edges parallel to and perpendicular to its straining axes (see #3 in Table 1). This upheaval of the whole indented region by the average compressive stress makes the additive pile-up along individual stress axis uncertain, thereby reducing the response rate in the asymmetric pile-up compared to the change in the stress ratio. In addition the material pile-up, formed by the plastic deformation process, inherently has a smaller variation range than the ratio of axial stress components in an elastic region. By expanding these arguments, the pure shear stress state or #4 can be taken as a combination of two orthogonal uniaxial stresses in opposite signs and its negligible pile-up variations can be explained by a large compensation of upward and downward surface displacements, respectively, occurred by the average compressive and tensile stresses. By taking into account the displacement resolution 0.3 μm of the laser microscope as a profile measuring error, an uncertainty of the ratio of the pile-up height shifts is calculated and overlapped on Fig. 5 as two dotted lines. A deviation behavior of the error bounds from the linear fitting line increases as κ approaches to -1.0. It means that a stress ratio of API X65 steel specimen in an arbitrary stress state can be predicted using Fig. 5, although a careful pile-up measurement must be carried out to establish the relationship between $\Delta h_y^{\text{pile}}/\Delta h_x^{\text{pile}}$ and κ.

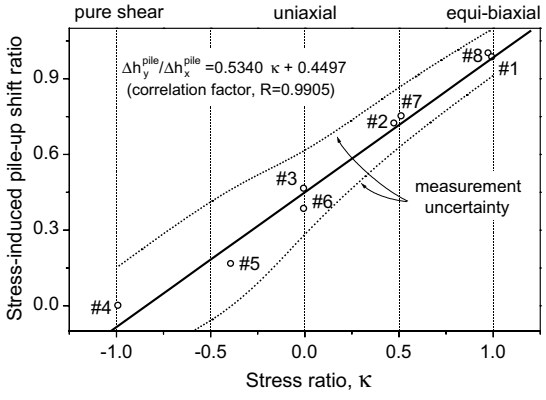

Fig. 5. A linear dependency of the two axial stress-induced pile-up shift ratio on the stress ratio.

4. Summary

An initiative study is done on the ratio prediction of two principal components in a biaxial surface stress through conical Brale indentations on artificial stresses simulated on steel specimens. A stress dependency of remnant impression morphology is investigated by measuring the variations in pile-up heights along two principal axes by the biaxial stress application. As a result, the ratio of stress-induced pile-up shifts showed a linear proportional relationship with the stress ratio applied for API X65 steel specimen, although its change scope was nearly half of that of the stress ratio. Thus this technique shows the application possibility of pile-up parameter for detecting the stress ratio but still has some limitations at present step, which will be the purposes of following studies. The changing rate of the pile-up parameter is too slow compared to that of the axial stress because pile-up deformation is susceptible to both the individual axial components and average of biaxial stress applied. The low sensitivity of the parameter also hindered its application for low surface stress with negative stress ratio. Furthermore a general function must be derived from the empirically fitted relationship through a theoretical model for the material pile-up behaviors in stressed and unstressed specimens.

Acknowledgment

This work was supported by the Post-doctoral Fellowship Program of Korea Science and Engineering Foundation (KOSEF).

References

[1] Sines G, Carlson R. ASTM Bull 1952;180:35.
[2] Vitovec FH. ASTM STP 889: Microindentation technique in materials science and engineering. Philadelphia: ASTM Publication; 1985. p. 175.
[3] Frenkel J, Abbate A, Scholz W. Exp Mech 1993;33:164.
[4] Tsui TY, Oliver WC, Pharr GM. J Mater Res 1996;11:752.
[5] Bolshakov A, Oliver WC, Pharr GM. J Mater Res 1996;11:760.
[6] Suresh S, Giannakopoulos AE. Acta Mater 1998;46:5755.
[7] Lee YH, Kwon D. Scripta Mater 2003;49:459.
[8] Swadener JG, Taljat B, Pharr GM. J Mater Res 2001;16:2091.
[9] Giannakopoulos AE. J Appl Mech 2003;70:638.
[10] Lepienski CM, Pharr GM, Park YJ, Watkins TR, Misra A, Zhang X. Thin Solid Films 2004;251–257:447.
[11] Lee YH, Kwon D. Acta Mater 2004;52:1555.
[12] Underwood JH. Exp Mech 1973;13:373.